GEOPHYSICAL RESEARCH LETTERS, VOL. 12, NO. 8, PAGES 514-517, AUGUST 1985

USE OF THE *PP* PHASE TO STUDY THE EARTHQUAKE SOURCE

Christopher S. Lynnes and Larry J. Ruff

Department of Geological Sciences, University of Michigan, Ann Arbor, MI 48109

Abstract. The space-time history of the rupture process of a large earthquake can be determined from directivity analysis of source time functions deconvolved from long-period *P* waves. However, such analysis requires a good azimuthal distribution of stations, which is often difficult to obtain. We have developed a method for deconvolution of long-period *PP* waves which is useful for a distance range of 70° - 123° and 145° - 165°, thus increasing both the available data and the ray parameter aperture. The *PP* waveform is Hilbert transformed to remove the effect of the *PP* caustic and then deconvolved in the time domain. We have tested the method on the 2 July 1974 Kermadec event (M_S=7.2) and obtained nearly identical source time functions from *P* and *PP* waves.

Introduction

Long-period *P* waves contain a great deal of information about the details of the rupture processes of large earthquakes. Deconvolution of the source time function from *P* waves yields the time-variant behavior of the earthquake (c.f., Ruff and Kanamori, 1983). Simultaneous deconvolution of several stations (Kikuchi and Kanamori, 1982) or deconvolutions coupled with directivity analysis (Beck and Ruff, 1984) or the Radon transform (Ruff, 1984) can define the spatial distribution of moment release. All three methods depend on the relative timing of source time function features as a function of the directivity parameter γ, where $\gamma = p \cos \phi$, p being the ray parameter and ϕ the difference of the fault and station azimuths. Thus, γ must be well sampled for adequate spatial resolution of the rupture process (e.g., Ruff, 1984). This condition is often difficult to meet, as when there are no stations in some azimuthal sector for teleseismic epicentral distances, particularly when the earthquake is too small to use stations further than 90° (i.e., diffracted *P* waves).

We have developed a method for deconvolving source time functions from *PP* waveforms; use of *PP* not only increases the amount of data available but can also improve azimuthal coverage by allowing the use of stations over a wider range of distances. The *PP* phase can be deconvolved at epicentral distances of 70° - 123° and 145° - 165°: closer than 70°, the *PP* phase is complicated by upper mantle structure; between 123° and 145°, the *PKS* phase interferes; and further than about 165°, the *PP* phase encounters the axial caustic. To deconvolve the *PP* waveform we must somehow account for the modifications of the direct *P* waveform introduced by the surface reflection and by the additional propagation. Although these modifications include greater attenuation and reverberations under the bounce point, the main change results from the internal caustic (Figure 1).

Paper number 5L6552.
0094-8276/85/005L-6552$03.00

Jeffreys and Lapwood (1957) have shown that the caustic introduces a constant $-\pi/2$ phase shift at high frequencies, which, when combined with the π phase shift from the free-surface reflection, gives a $\pi/2$ phase shift. Choy and Richards (1975) give an intuitive discussion of how the phase shift arises at a caustic and show actual examples of this phase shift in the analogous *SS* phase. The $\pi/2$ phase shift transforms a function into its inverted allied function (or inverse Hilbert transform), an example of which is shown for the Dirac delta function ($\delta(t)$) in Figure 1. The analytic form of the inverted allied function of $\delta(t)$ is $1/(\pi t)$ for $t \neq 0$ and 0 for $t=0$; thus, there is energy arriving both before and after the geometric arrival time. For an actual seismogram, both the earth transfer function and instrument are band-limited, and the band-passed inverted allied function simply has a small precursor and coda. By applying the Hilbert transform, Butler (1982) successfully modelled these features in *SS* waveforms from the 1973 Hawaii earthquake. In a theoretical study of the *PP* phase, Hill (1974) has shown that in some cases, the phase shift may be frequency-dependent, tending toward $\pi/2$ at high frequency and toward 0 at low frequency due to interaction with the surface. At sufficient distance, however (i.e., $\Delta > 70°$), even long-period *PP* waves should be free from this effect. Our technique for deconvolving the *PP* waveform consists simply of removing the $\pi/2$ phase shift introduced by the reflection at the surface and the internal caustic, and then deconvolving as we would a direct *P* waveform, allowing for differences in attenuation (i.e., doubling t*) and geometric spreading ($g(\Delta)$).

Data and Discussion

For our test case, we chose the 2 July 1974 earthquake in the Kermadec Islands (M_S=7.2). The event occurred at 29.22° S, 175.94° W, with an origin time of 23:26:26.8 (ISC). Chapple and Forsyth (1979) show a first-motion focal mechanism with fault azimuth 65°, dip 22°, and slip angle 137° (Figure 2). Preliminary deconvolutions of the *P* and diffracted *P* waves indicate a shallow focal depth of 0-20 km (D. Christensen, pers. comm.), which is also implied by the absence of discernible

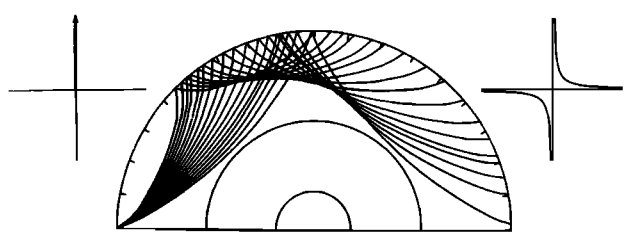

Fig. 1. Ray tracing of *PP* through spherically symmetric earth model. *PP* emerges at distances from 90° to 180°. The *P* wave arrival is represented by the impulsive delta function (left) while the *PP* phase is the inverted allied function (right).

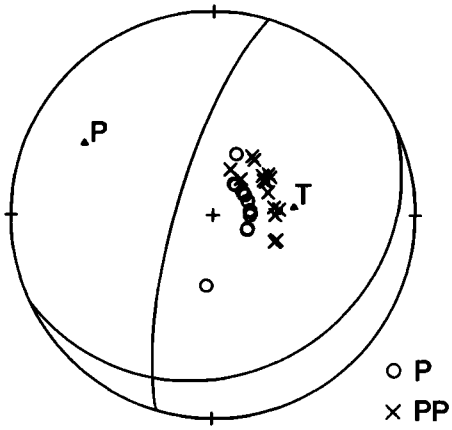

Fig. 2. Equal area projection on the lower hemisphere of the focal mechanism for 2 July 1974 Kermadec event. The locations of the *P* (circles) and *PP* phases (crosses) used in this study are plotted on the focal sphere. Triangles are the pressure (P) and tension (T) axes.

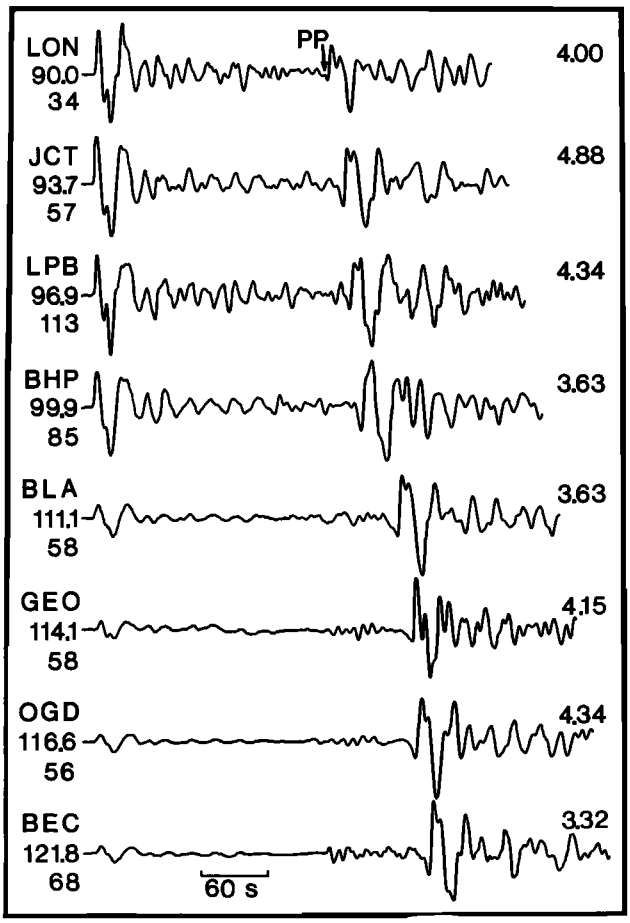

Fig. 3. Distance profile of *P* and *PP* waveforms for eight stations. Station code, epicentral distance (deg.), and event-station azimuth (deg.) are listed to the left of each seismogram, with the maximum peak-to-peak amplitude (cm) to the right. While the amplitude of the *P* wave decreases in the shadow zone, *PP* maintains a relatively constant amplitude.

depth phases. The phases used are plotted on the focal sphere in Figure 2. The abundance of stations in the same azimuth with distance range 90° - 122° and the simplicity of the direct *P* waves (Figure 3) were the primary reasons for the selection of this event as our test case. The small, emergent precursors of the *PP* phases in Figure 3 are typical of the phase, as are the nearly constant *PP* amplitudes in the range of 90° - 122°.

Our first test was to see whether the *PP* phases are in fact the inverse Hilbert transforms of the direct *P* phases. We digitized the waveforms from ten seconds before the direct *P* arrival to at least three minutes past the *PP* arrival; the seismograms were then interpolated at a time interval of 0.2 seconds. We then applied the Hilbert transform to the whole waveform using the frequency-domain procedure of Choy and Richards (1975). The 10 second leader is necessary because of the precursor energy which arises when the Hilbert transform is applied. The Hilbert transform of the seismogram at LON is shown below the seismogram itself in Figure 4. For a successful test, the Hilbert transform of *PP* should be similar (neglecting the difference in takeoff angle) to the direct *P*, while the Hilbert transform of the *P* should be the inverse of the observed *PP*. Clearly, the wave shapes match extremely well. Note also that the impulsive nature of the direct *P* is recovered in the *PP* by the application of the Hilbert transform, thus allowing an accurate pick of the *PP* arrival time.

Next we compared source time functions deconvolved from *P* and diffracted *P* waves with those deconvolved from the Hilbert transforms of *PP* waves. Our deconvolution technique is a time-domain damped Lanczos inverse (Ruff and Kanamori, 1983). We used a focal depth of 10 km, a t* of 1.0 for *P*, *pP*, and *sP* and a t* of 2.0 for *PP*, *pPP*, and *sPP*. The records were deconvolved at a time interval of 2 seconds, with a damping of 0.01. The geometric spreading factors for *P* are taken from Kanamori and Stewart (1976), with all stations greater than 90° assigned a factor of 0.25. The geometric spreading factor predicted by simple geometric ray theory for *PP* is given by $1/2\ [\cos(\Delta/2)]^{-1/2}\ g(\Delta/2)$, where $g(\Delta/2)$ is the geometric spreading factor for a *P* wave at half the epicentral distance. This formula gives a nearly constant spreading factor of 0.25

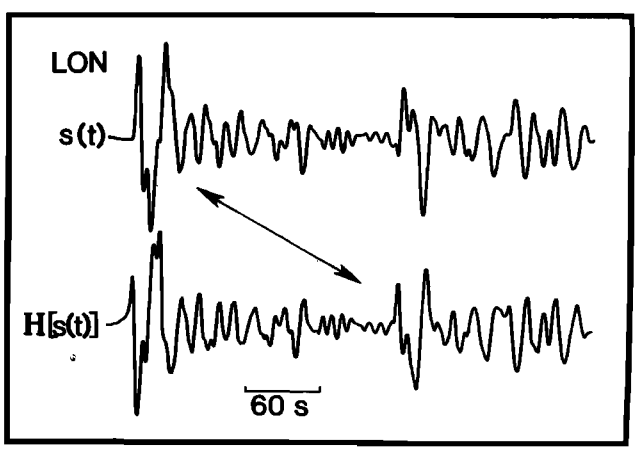

Fig. 4. Seismogram from LON plotted above its Hilbert transform at the same scale. Note the strong correspondence between the *P* waveform and the transformed *PP* waveform.

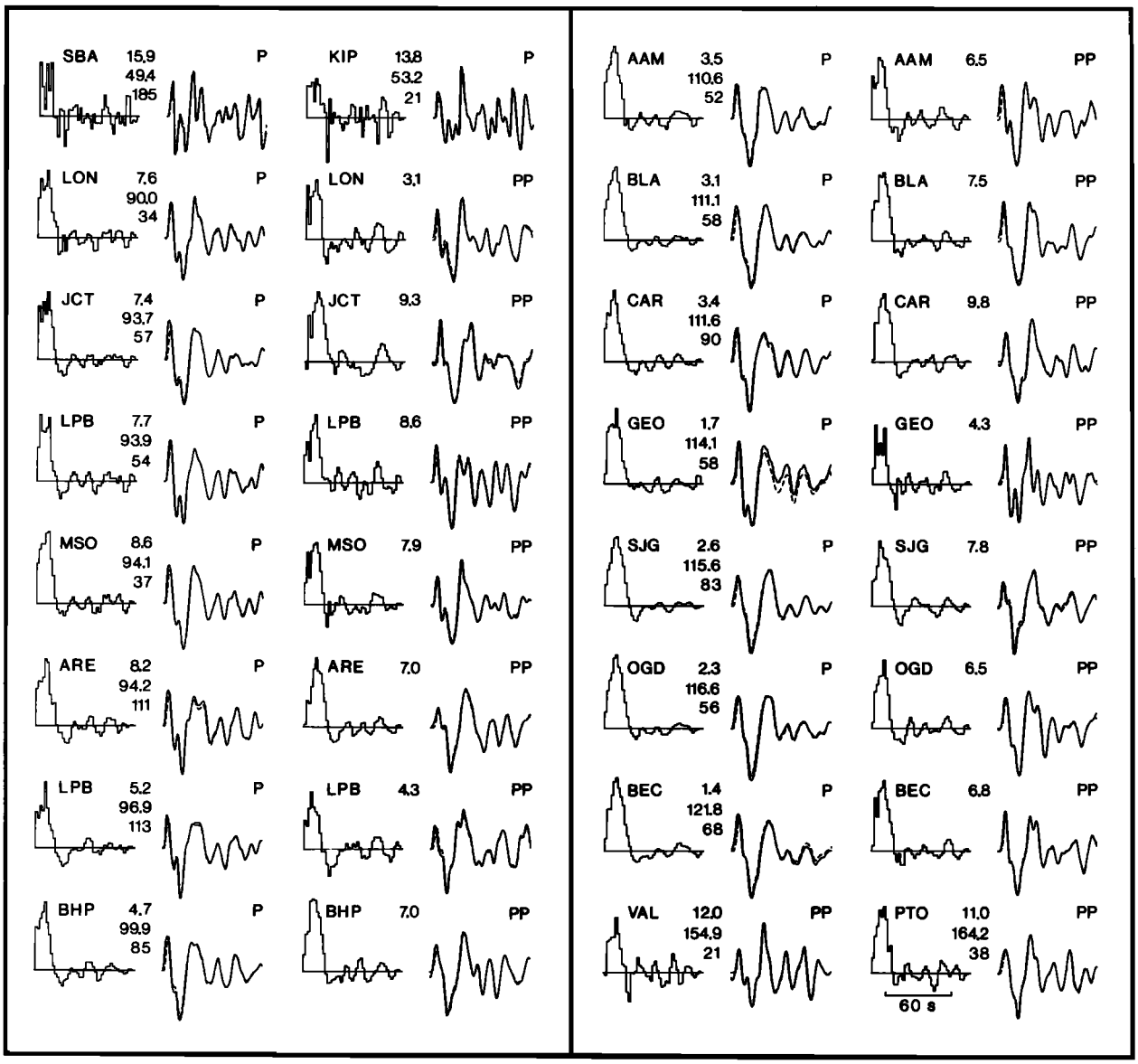

Fig. 5. Source time functions deconvolved from *P* and *PP* phases, in order of increasing epicentral distance. *P* wave source functions are plotted to the left of the observed (solid line) and synthetic (dashed line) *P* wave seismograms. *PP* source functions are to the left of the Hilbert transforms of the observed (solid line) and synthetic (dashed line) seismograms. The *P* and *PP* phases from a station are plotted beside each other. Station code, seismic moment (in 10^{26} dyne-cm), distance and azimuth (deg.) are listed for each source function, with the phase indicated on the right. Stations LON through BEC have source functions from both phases, which show a strong correlation.

in the range 90° - 122°, which is consistent with the small variation in the observed amplitudes. Although all of the midpoints of the *PP* phases used in this study are oceanic, the effects of water bounces at the midpoint were neglected due to the long periods of the waveforms considered here.

The resulting source time functions are shown in Figure 5, with the source time functions from the transformed *PP* phase plotted aside those deconvolved from the *P* (or diffracted *P*) phase at the same station; the exceptions are SBA (Δ=49.4°) and KIP (Δ=53.2°), which are too close for *PP*, and VAL (Δ=154.9°) and PTO (Δ=164.2°), which are too far for diffracted *P*. The basic source time function as indicated by the diffracted and direct *P* waves is a single 18-second pulse, with an apparent seismic moment of about 8 x 10^{26} dyne-cm. As with the observed waveforms and their Hilbert transforms, the correspondence between the time functions from *P* and *PP* is quite remarkable. In fact, the *PP*-derived source time functions show no more noise than those from *P* and diffracted *P*, justifying the neglect of water bounces. Furthermore, the seismic moments derived from the *PP* deconvolutions are fairly consistent. The mean moment from the *PP* waveforms is 7.5 ($\pm$2.4) x 10^{26} dyne-cm, very close to the moment derived

from the direct *P* phases. Thus, it appears that the geometric spreading factors from simple geometric ray theory adequately predict both the relative and absolute amplitudes.

Conclusion

We have used a simple large earthquake to show that the long-period characteristics of the *PP* phase are easily modeled, and that the source time function can be deconvolved from the *PP* waveform. The chief advantages of the *PP* phase are: 1) *PP* phases arriving at all distances are undiffracted; and 2) the ray parameter of a given *PP* phase is that of the *P* phase at half the distance. The first feature allows both the reliable determination of seismic moments from seismograms recorded at stations greater than 90° from the source and the use of stations whose diffracted *P* waves are too small. The second feature increases the range in ray parameter, and thus directivity parameter, which can be sampled. It may also help in the study of vertical strike-slip events (or dip-slip events with a steep plane), where stations corresponding to steep takeoff angles are near-nodal. Most importantly, perhaps, *PP* deconvolution augments the available data set for a given earthquake. This is particularly crucial for earthquakes before 1963, where few seismograms are generally available for a given event.

Acknowledgements. We thank D. Christensen for providing the results of his preliminary deconvolutions, and T. Lay, S.L. Beck and S.Y. Schwartz for several helpful comments and suggestions. This research was supported by grants from the National Science Foundation (P.Y.I./EAR-8351515 and EAR-407786) and the Shell Companies Foundation to L.J.R. One author (C.S.L.) was also supported by a Rackham Fellowship.

References

Beck, S.L., and L.J. Ruff, The rupture process of the great 1979 Colombia earthquake: evidence for the asperity model, *J. Geophys. Res., 89,* 9281-9291, 1984.

Butler, R., The 1973 Hawaii earthquake: a double earthquake beneath the volcano Mauna Kea, *Geophys. J. R. Astr. Soc., 69,* 173-186, 1982.

Chapple, W. M. and D.W. Forsyth, Earthquakes and bending of plates at trenches, *J. Geophys. Res., 84,* 6729-6749, 1979.

Choy, G.L. and P.G. Richards, Pulse distortion and Hilbert transformation in multiply reflected and refracted body waves, *Bull. Seismol. Soc. Am., 65,* 55-70, 1975.

Hill, D.P., Phase shift and pulse distortion in body waves due to internal caustics, *Bull. Seismol. Soc. Am., 64,* 1733-1742, 1974.

Jeffreys, H. and E.R. Lapwood, The reflection of a pulse within a sphere, *Proc. Roy. Soc., Ser. A, 241,* 455-479, 1957.

Kanamori, H. and G.S. Stewart, Mode of the strain release along the Gibbs fracture zone, Mid-Atlantic Ridge, *Phys. Earth Planet. Int., 11,* 312-332, 1976.

Kikuchi, M., and H. Kanamori, Inversion of complex body waves, *Bull. Seismol. Soc. Am., 72,* 491-506, 1982.

Ruff, L.J., Tomographic imaging of the earthquake rupture process, *Geophys. Res. Lett., 11,* 629-632, 1984.

Ruff. L., and H. Kanamori, The rupture process and asperity distribution of three great earthquakes from long-period diffracted *P* waves, *Phys. Earth Planet. Int., 31,* 202-230, 1983.

(Received April 23, 1985;
accepted May 15, 1985.)